

LA-UR-21-27882

Approved for public release; distribution is unlimited.

Title: Re-calibration of PBX9501 SURF model

Author(s): Menikoff, Ralph

Intended for: Report

Issued: 2021-08-06

Disclaimer:

Los Alamos National Laboratory, an affirmative action/equal opportunity employer, is operated by Triad National Security, LLC for the National Nuclear Security Administration of U.S. Department of Energy under contract 89233218CNA000001. By approving this article, the publisher recognizes that the U.S. Government retains nonexclusive, royalty-free license to publish or reproduce the published form of this contribution, or to allow others to do so, for U.S. Government purposes. Los Alamos National Laboratory requests that the publisher identify this article as work performed under the auspices of the U.S. Department of Energy. Los Alamos National Laboratory strongly supports academic freedom and a researcher's right to publish; as an institution, however, the Laboratory does not endorse the viewpoint of a publication or guarantee its technical correctness.

RE-CALIBRATION OF PBX9501 SURF MODEL

RALPH MENIKOFF

July 29, 2021

1 Introduction

PBX 9501 is a plastic bonded explosive composed of 95 wt % HMX and a binder; see [Gibbs and Popolato, 1980, pp. 109–119]. SURF is a reactive burn model for shock initiation and propagation of detonation waves. It has previously been calibrated for PBX 9501.

Here the SURF model is recalibrated for PBX 9501; specifically, lot 730-010 at $\rho = 1.837 \text{ g/cc}^3$. The new calibration uses the Davis reactants and products EOS calibrated for the AWS model [Aslam et al., 2020]. The burn rate in the shock initiation regime is fit to the Pop plot from 5 embedded gauge shock-to-detonation transition (SDT) experiments from [Gustavsen et al., 1999, see fig 12 and table 5]. In the propagation regime, the burn rate is fit to curvature effect data (detonation speed as function of front curvature); see [Aslam, 2007].

Also the burn parameters are adjusted to fit the gap-stick experiment [Hill et al., 2018]. Simulating the detonation wave speed in this experiment requires a model that is accurate for initiation with complex shock loading; in particular, a pressure decreasing gradient behind a curved lead shock. This is more difficult than calibrating to the standard SDT experiments which are 1-D and driven by a sustained shock. Simulations of the gap-stick experiment for PBX 9501 with the SURF model will be discussed in a subsequent report.

The curvature effect for PBX 9501 is small and requires a narrow reaction-zone width for a propagating detonation wave. A rate parameter needed to fit initiation with a pressure gradient behind the lead shock, as occurs in the gap-stick experiment, couples to the detonation regime and causes the rate in the detonation regime to be too small to obtain a sufficiently narrow reaction-zone width to fit the curvature effect. To circumvent this issue and better decouple burn rate parameters for the initiation and propagation regimes, an option is added to the fitting form for the SURF burn rate and is used in the re-calibration. The new option is described in Appendix A.

Simulations for the calibration use the xRage code. Its adaptive mesh refinement (AMR) capability allows the narrow reaction zone of a propagating detonation wave to be adequately resolved more efficiently than with a uniform mesh.

2 PBX 9501 EOS

Previous the SURF model was calibrated to PBX 9501 using sesame tables for the reactants and products EOS. When the sesame products table was extended to have a larger domain, a 1 percent error was inadvertently introduced into the CJ detonation speed. The SURF burn rate was recalibrated with a Davis EOS for the reactants and products with parameters from [Aslam et al., 2020, tables I and II] used for the AWS model. The CJ detonation wave states for the model EOS with initial density 1.836 g/cc are listed below:

Initial reactants state							
5.4466e-01	0.0000e+00	0.0000e+00	1.0000e-04	2.3000e+00	2.3000e+00	6.6868e+00	2.9700e+02
VN spike state							
2.9966e-01	7.8540e+00	3.9633e+00	6.4115e+01	8.8110e+00	7.7576e+00	1.3388e+00	3.0358e+03

V	e	u	P	us	c	FD	T
cm ³ /g	MJ/kg	km/s	GPa	km/s	km/s		K

CJ products state							
4.1130e-01	2.3272e+00	2.1574e+00	3.4900e+01	8.8110e+00	6.6536e+00	2.0076e+00	3.6369e+03

The shock locus, detonation locus and the CJ release isentrope are shown in fig. 1.

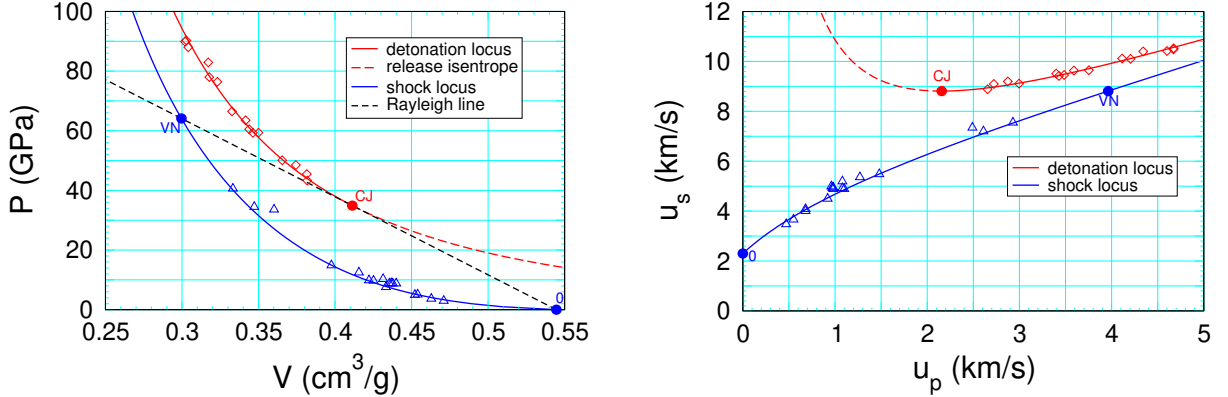


Figure 1: Shock and detonation loci for PBX 9501 from model EOS; (V, P) -plane on left and (u_p, u_s) -plane on right. The triangle symbols are data points.

Note that the VN spike pressure and temperature are slightly high compared to previous calibration, which in turn are high compared to other PBX 9501 EOS models. High pressure reactants shock data is problematic due to the high burn rate behind the shock. (The 3 highest pressure points in the figure are for single crystal HMX, which due to the lack of pores, and hence hot spots, have a lower burn rate than that of the PBX.) The high pressure Davis EOS model is constrained such that the reactants shock locus and the products detonation locus do not intersect. Since reactive burn models are empirical, to a large extent, the calibration of the rate can compensate for inaccuracies in the EOS.

Also of interest is the sonic pressure on the shock polar with the incoming particle velocity set to the detonation speed. This is the boundary condition for the lead shock in an unconfined rate stick. For the Davis reactants EOS, the sonic pressure is 32 GPa. This is surprisingly high; only slightly less than the CJ pressure of 35 GPa.

3 SURF rate and ZND profile

The SURF burn rate has the form

$$\lambda = g(s) , \quad (1a)$$

$$\frac{d}{dt}s = \tilde{\mathcal{R}}(p_s, p) = f(p_s) \cdot \begin{cases} 0 & \text{for } p \leq 0 , \\ \left[\frac{p}{p_s}\right]^n & \text{for } 0 < p < p_s , \\ \left[\frac{p}{p_s}\right]^{n_{hi}} & \text{for } p_s \leq p , \end{cases} \quad (1b)$$

where λ is the SURF reaction progress variable (mass fraction of products), s is a scaled reaction variable, p_s is the lead shock pressure and p is the local pressure. The fitting forms and parameters for the reaction scale function $g(s)$ and the rate function $f(p_s)$ are specified in the xRage users manual and [Menikoff, 2017, App. A]. The standard burn rate is $d\lambda/dt = (dg/ds) \cdot \tilde{\mathcal{R}}(p_s, p)$ where dg/ds depends only on λ since $g(s)$ is monotonic and hence invertible.

Below the CJ pressure, the SURF rate function $f(p_s)$ is calibrated to Pop plot data and embedded velocity gauge data from shock-to-detonation transition (SDT) experiments. The parameter n_{hi} affects the shape of the velocity time histories. The parameter n is intended to help fit shock initiation with a pressure decreasing gradient behind the shock front. It is adjust to better fit the gap-stick experiment [Menikoff, 2021]. The PBX 9501 calibration uses $n = 2.5$ and $n_{hi} = 1.5$.

In the high pressure propagation regime, the SURF rate parameters are fit to curvature effect data; *i.e.*, detonation speed as a function of front curvature, $D_n(\kappa)$. The curvature effect is strongly dependent on the reaction-zone width. The parameter n lowers the rate and increases the reaction-zone width. Parameters coupling to both the initiation and propagation regimes make calibrating the rate more difficult. To eliminate the unintended effect of n on the propagation regime, a cutoff on the pressure ratio factor in the rate Eq. (1b) has been added to the SURF rate model. This is described in Appendix A.

The calibrated PBX 9501 rate parameters are listed in Appendix B. For these parameters, the rate function $f(p_s)$ is shown in fig. 2. With the pressure ratio cutoff, the reaction zone or ZND profile for a planar detonation wave is determined by the rate functions $f(p_s)$ and $g(s)$; *i.e.*, in effect $n = n_{hi} = 0$ in the detonation regime. The profiles versus distance and time for are shown in fig. 3. The reaction-zone width is 0.057 mm and reaction time is 0.010 μ s.

Numerical profiles are shown in fig. 4 for 3 resolutions. To resolve the reaction zone, a cell size of 0.004 mm is needed. At a cell size of 0.016 mm, there is substantial burning in the shock rise, and the numerical wave width to the CJ pressure is noticeably larger. At 0.064 mm, truncation errors cause the sonic (CJ) state to occur after the reaction is complete, and leads to a numerical wave width significantly too large. Nevertheless, the CJ pressure and the release wave are not sensitive to the resolution. High resolution is needed to accurately reproduce the curvature effect and the shape of the detonation front. For low resolution, the speed of a curved detonation wave may be a couple of percent low. For shock initiation, the burn rates are much lower than in the reaction zone of a detonation wave and the needed resolution is much lower. The SDT calibration simulations discussed in the next section use AMR with cell size down to 0.016 mm.

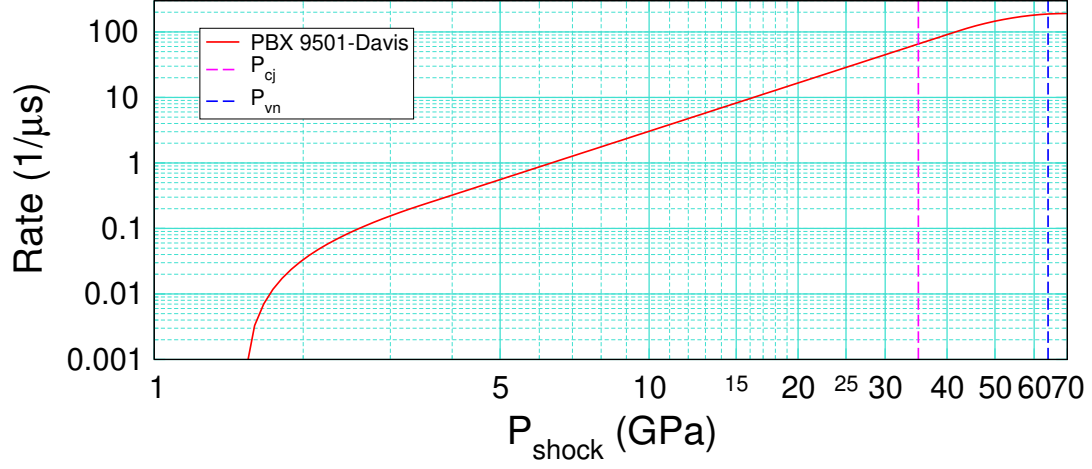


Figure 2: SURF rate function $f(p_s)$ for PBX 9501.

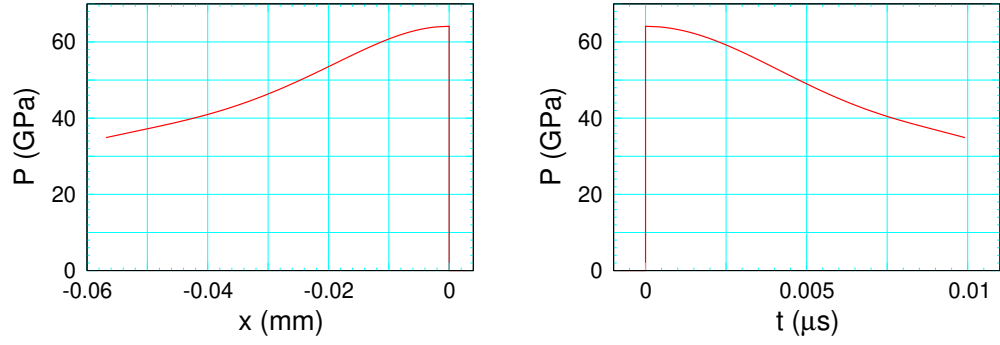


Figure 3: CJ detonation wave profiles for SURF model of PBX 9501. Pressure vs distance at fixed time on left, and Lagrangian pressure time history on right.

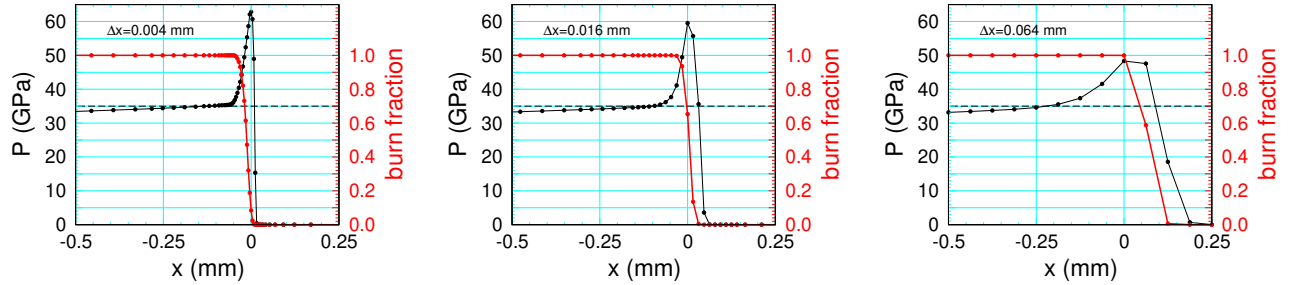


Figure 4: Detonation wave reaction-zone profiles of pressure and reaction progress variable from 1-D simulations of a propagating detonation wave for cell sizes of 4, 16 and 64 microns. Symbols correspond to cells. Dashed line is at the CJ pressure (35 GPa).

4 Pop plot and velocity gauge data

PBX 9501 can be pressed to densities between 1.833 and 1.844 g/cc. Below 7 GPa there are measurable differences in the Pop plot with initial density and lot. The calibration in the initiation regime calibration is based on Pop plot derived by [Gustavsen et al. \[1999, fig 12 and table 5\]](#)

$$\text{Distance of run:} \quad \log_{10}(x/\text{mm}) = 1.94 - 1.66 \log_{10}(P/\text{GPa}),$$

$$\text{Time to detonation:} \quad \log_{10}(t/\mu\text{s}) = 1.52 - 2.00 \log_{10}(P/\text{GPa}),$$

and embedded velocity gauge data for lot 730-010 at 1.837 g/cc.

The initial shock pressure for Pop plot data points from SDT experiments is based on the impedance match of the projectile impacting the PBX. This uses EOS for the projectile material and reactants derived from previous measurements; see [[Gustavsen et al., 1999](#), table 2, fig 2 and §calculation of impact stresses]. Using the Davis reactants EOS, the initial pressure from the impedance match would differ by a few percent. Consequently, the rate parameters based on the Pop plot are adjusted to better fit the lead shock trajectory from the SDT experiments.

Even though [Gustavsen et al. \[1999\]](#) did a large number of PBX 9501 experiments, they covered different densities and different lots. For lot 730-010 at 1.837 g/cc, there were only 5 shots: 1s1144, 1s1145, 1s1146, 1s1147, 1s1150. There are 2 pairs of shots that are near duplicates; 1s1144 and 1s1145 at shock pressure of 5.2 GPa (vital projectile with velocities of 0.816 and 0.811 km/s, respectively), and 1s1146 and 1s1147 at 3.1 GPa (z-cut-quartz projectile with velocity of 0.652 and 0.651 km/s, respectively).

Figure 5 shows a comparison of the shock trajectories for each pair. The projectile velocities are close enough that the simulated trajectories with the calibrated SURF model are barely distinguishable. The experimental trajectories before transition to detonation are also nearly the same. After transition there is a time shift of (25 to 80 ns). This is due to a small shift in the transition point (up to 0.5 mm). It indicates that different PBX samples can have small variations in burn rate, presumably due to statistical variations in the PBX heterogeneities. The shift in the transition point with PBX sample would give an uncertainty in Pop plot data points of up to a few percent.

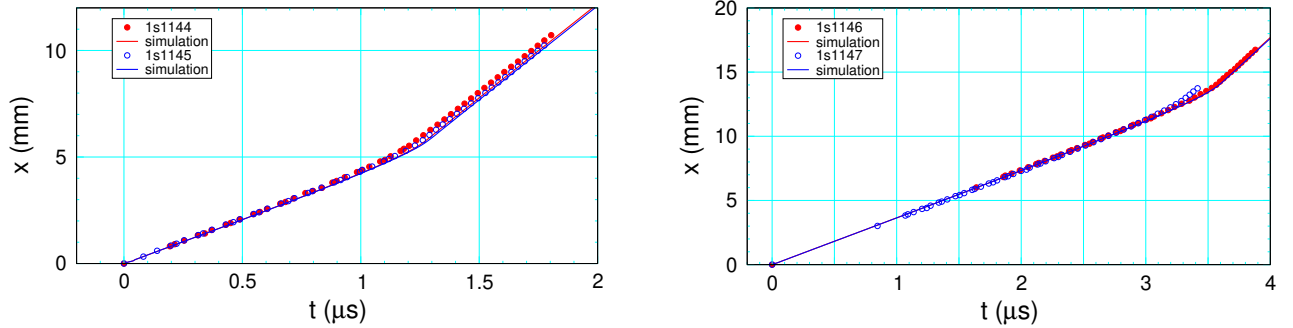


Figure 5: Comparison of lead shock trajectories for shots 1s1144 and 1s1145 and for shots 1s1146 and 1s1147.

A comparison of velocity gauge profiles at similar positions for the 2 pairs of duplicate shots are shown in fig. 6. The corresponding profiles are similar in shape and amplitude but not exactly the same. Part of the difference is due to a slight difference in corresponding gauge position. There also can be small differences in the response of the gauges on different shots.

Overall the reproducibility of the gauge data is good. Simulated and experimental gauge data can be expected to have some differences. For the SURF model, the shape of the simulated gauge profiles depends largely on the pressure ratio factor in Eq. (1b) and on the λ dependence of the burn rate; *i.e.*, reaction scale function $g(s)$.

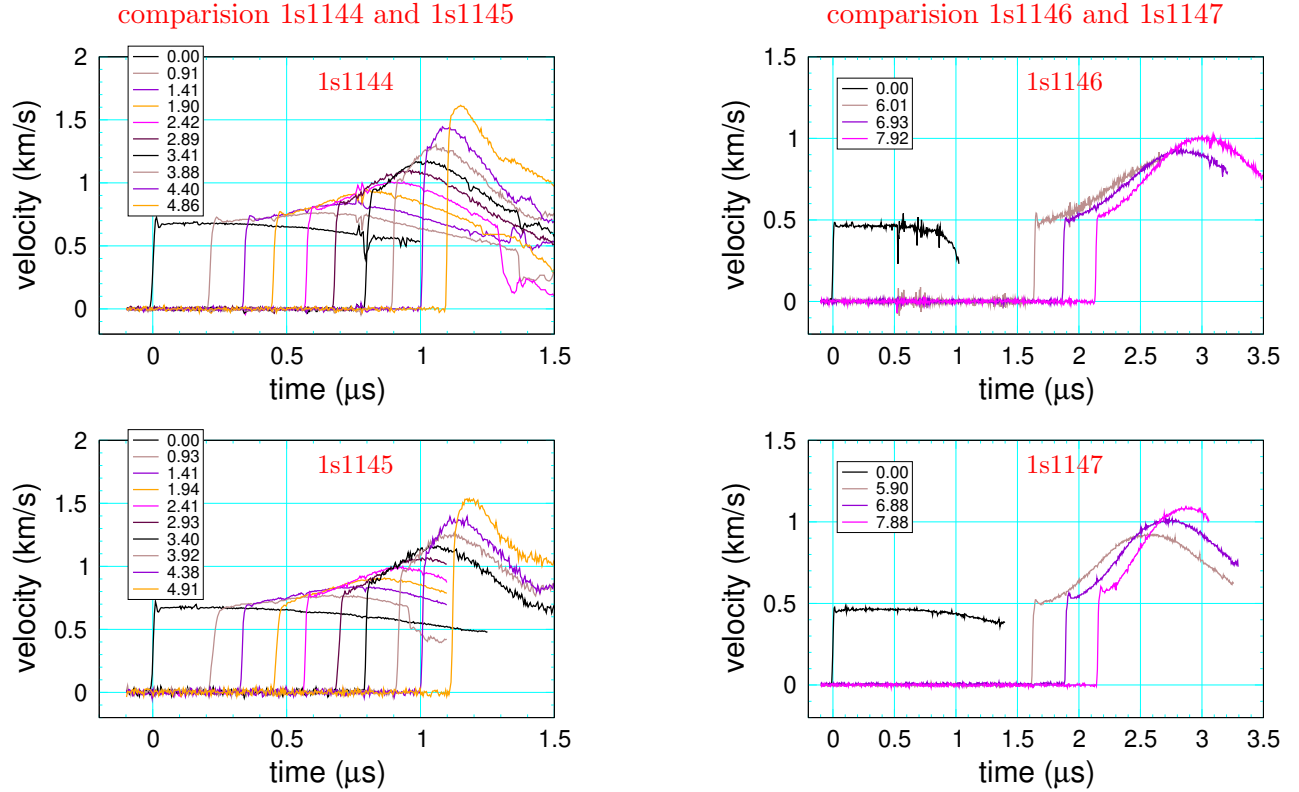


Figure 6: Comparison of velocity gauge profiles, at nearly the same positions, for shots 1s1144 and 1s1145 and for shots 1s1146 and 1s1147.

4.1 shot 1s-1144 ($P_s = 5.21$ GPa)

A comparison of experimental and simulated gauge data for shot 1s-1144 is shown in fig. 7. The profile of the last embedded velocity gauge is characteristic of a detonation wave. It is consistent with the transition shown in the tracker gauge trajectory; *i.e.*, abrupt change in slope. The simulated transition is a little late which results in a time shift after transition in the comparison with the tracker gauges.

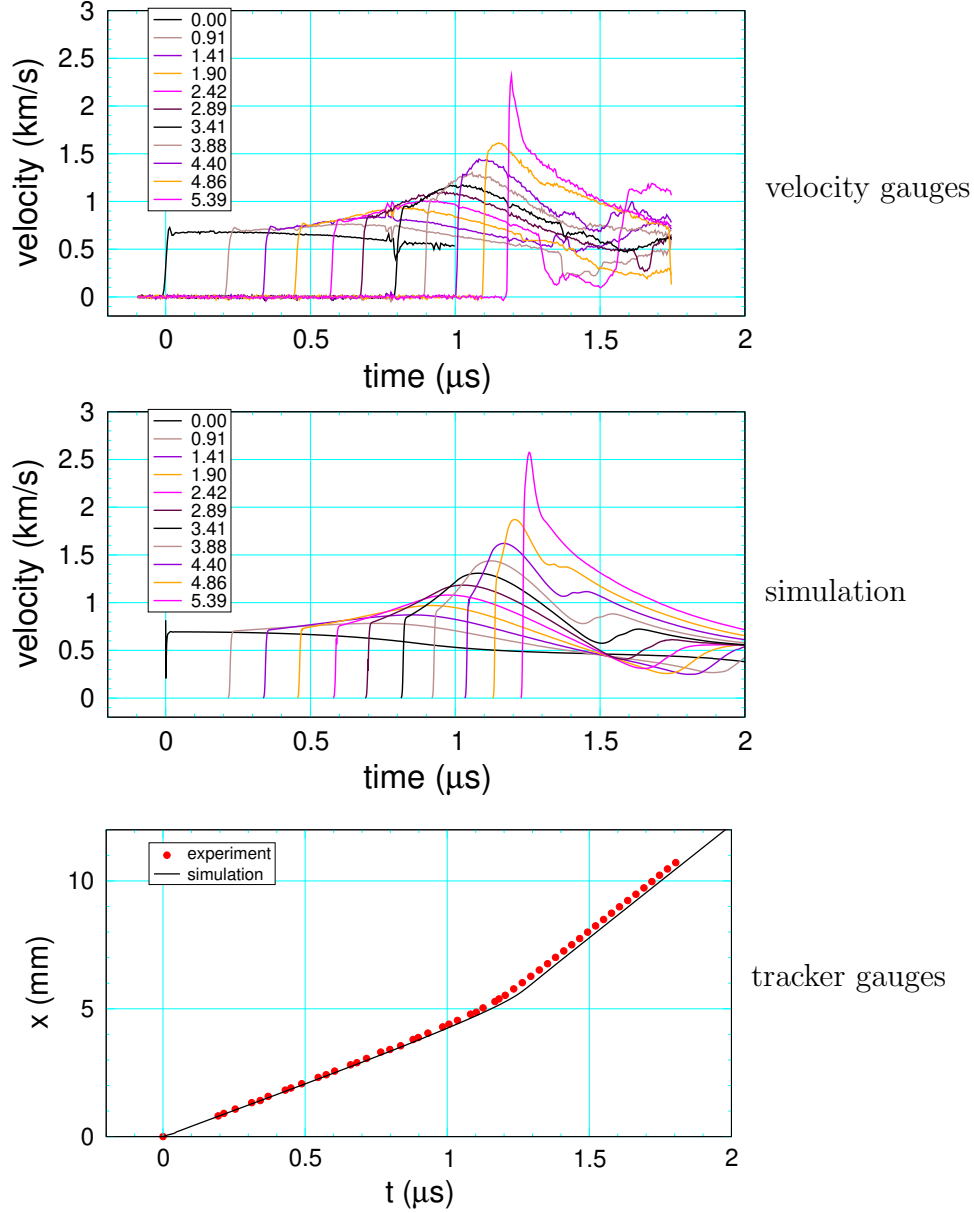


Figure 7: Comparison for shot 1s-1144 between experimental data [Gustavsen et al., 1999] and SURF model simulation. Top and middle plots for embedded velocity gauge data (legend labels gauge position in mm) and bottom plot for lead shock trajectory.

4.2 shot 1s-1145 ($P_s = 5.17$ GPa)

A comparison of experimental and simulated gauge data for shot 1s-1145 is shown in fig. 8. The embedded velocity gauges only show the build up of the lead shock, as they were not positioned far enough downstream to display a detonation profile. The transition is seen in the tracker gauges. The simulated transition is a little late which results in a time shift after transition in the comparison with the tracker gauges.

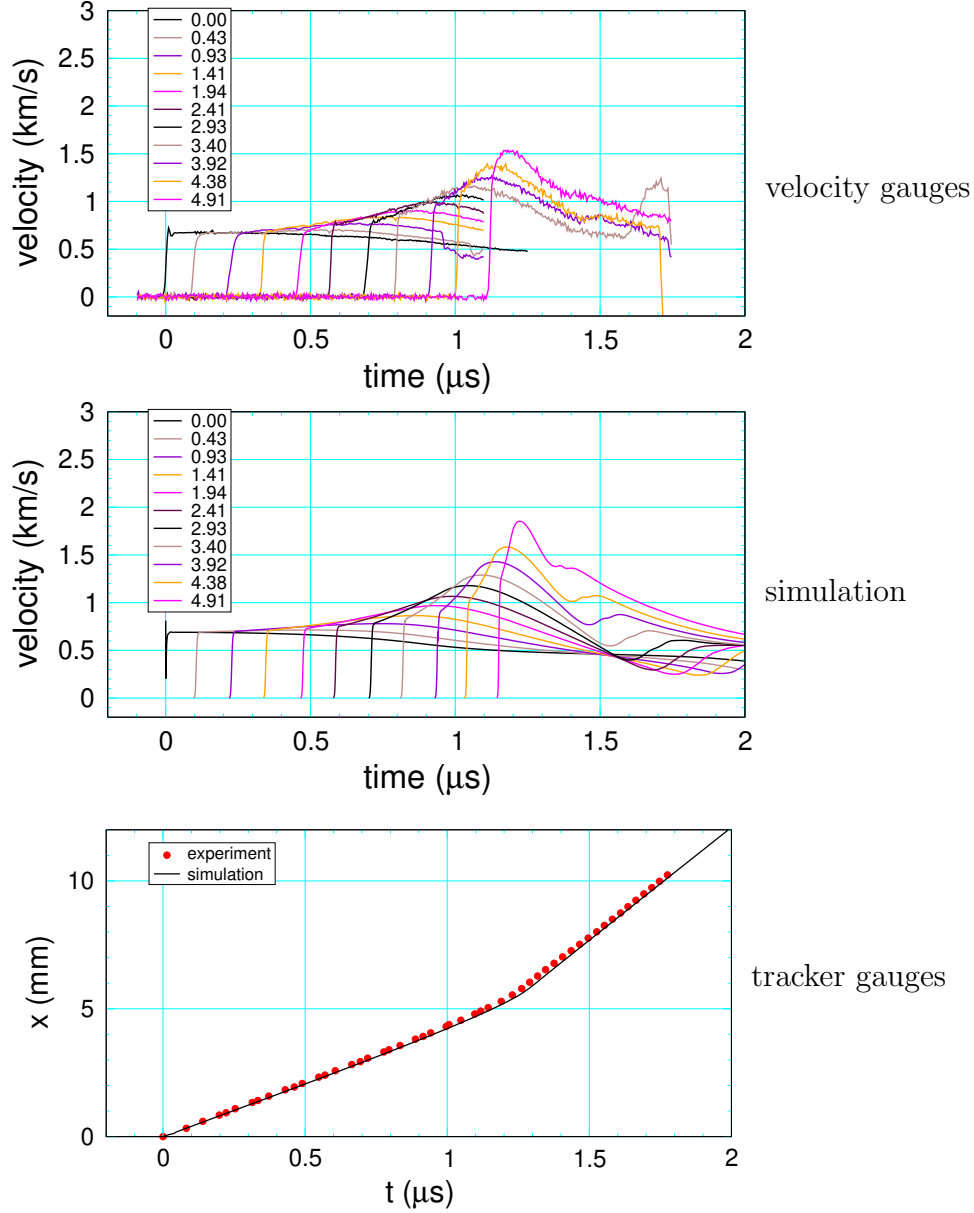


Figure 8: Comparison for shot 1s-1145 between experimental data [Gustavsen et al., 1999] and SURF model simulation. Top and middle plots for embedded velocity gauge data (legend labels gauge position in mm) and bottom plot for lead shock trajectory.

4.3 shot 1s-1150 ($P_s = 3.90$ GPa)

A comparison of experimental and simulated gauge data for shot 1s-1150 is shown in fig. 9. The embedded velocity gauges only show the build up of the lead shock, as they were not positioned far enough downstream to display a detonation profile. The transition is seen in the tracker gauges. The simulated and experimental lead shock trajectory are in good agreement.

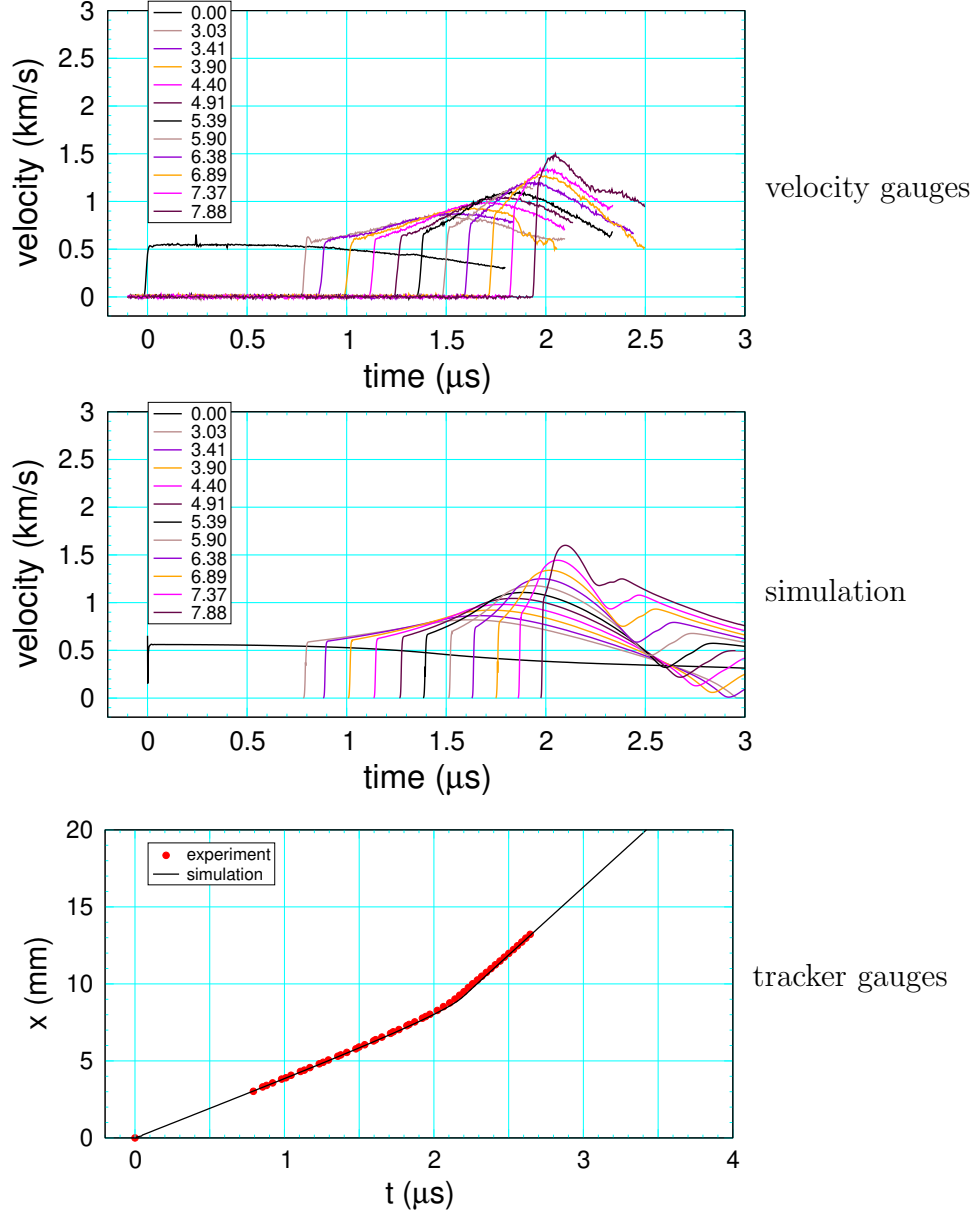


Figure 9: Comparison for shot 1s-1150 between experimental data [Gustavsen et al., 1999] and SURF model simulation. Top and middle plots for embedded velocity gauge data (legend labels gauge position in mm) and bottom plot for lead shock trajectory.

4.4 shot 1s-1146 ($P_s = 3.10$ GPa)

A comparison of experimental and simulated gauge data for shot 1s-1146 is shown in fig. 10. The embedded velocity gauges only show the build up of the lead shock, as they were not positioned far enough downstream to display a detonation profile. The transition is seen in the tracker gauges. The simulated and experimental lead shock trajectory are in good agreement.

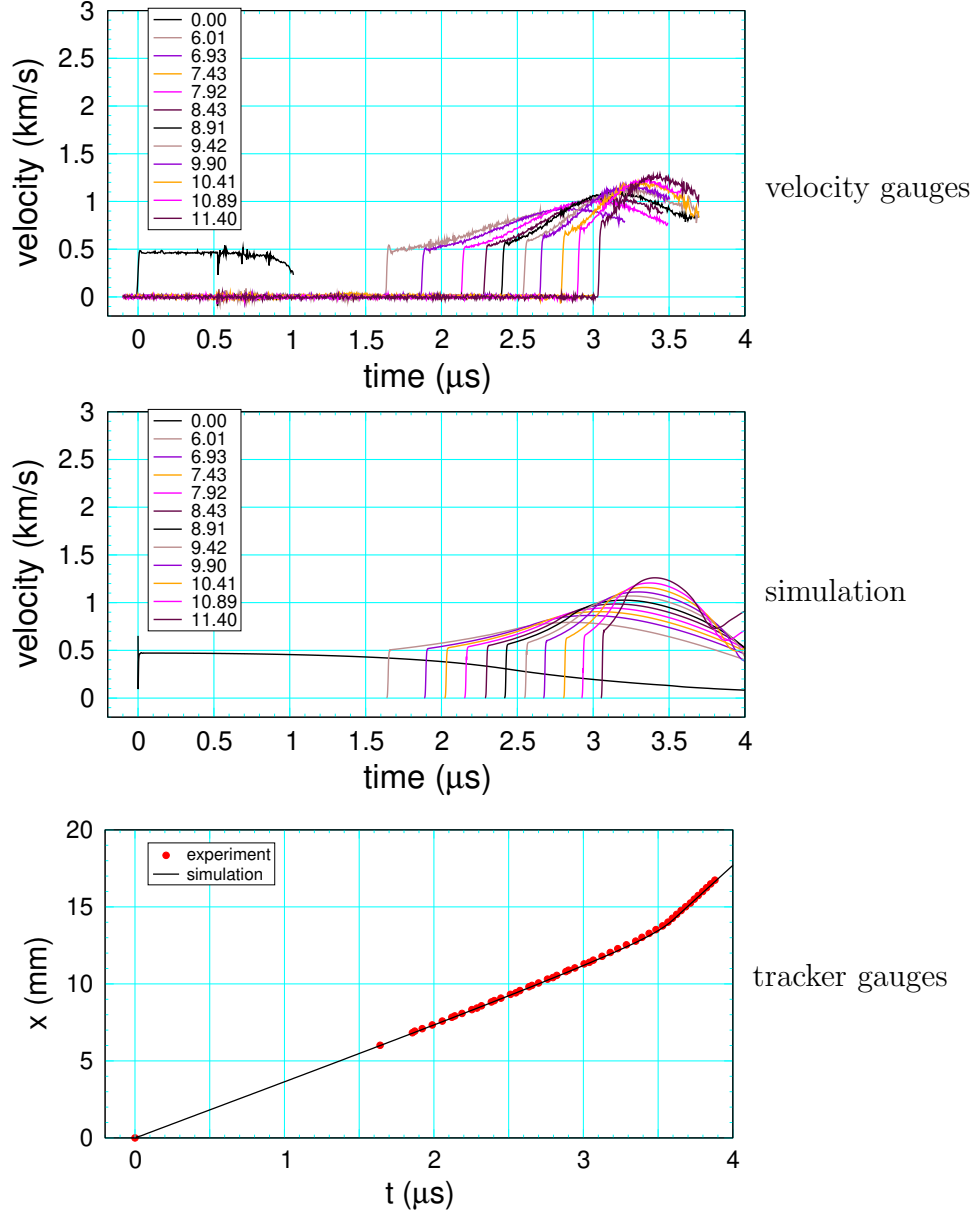


Figure 10: Comparison for shot 1s-1146 between experimental data [Gustavsen et al., 1999] and SURF model simulation. Top and middle plots for embedded velocity gauge data (legend labels gauge position in mm) and bottom plot for lead shock trajectory.

4.5 shot 1s-1147 ($P_s = 3.10$ GPa)

A comparison of experimental and simulated gauge data for shot 1s-1147 is shown in fig. 11. The embedded velocity gauges only show the build up of the lead shock, as they were not positioned far enough downstream to display a detonation profile. The start of the transition is seen in the tracker gauges. The simulated transition in the tracker gauges is late. As discussed in the start of this section, shot 1s-1147 is a near duplicate of shot 1s-1146. The difference in the transition point is due to variation of the burn rate with different PBX samples.

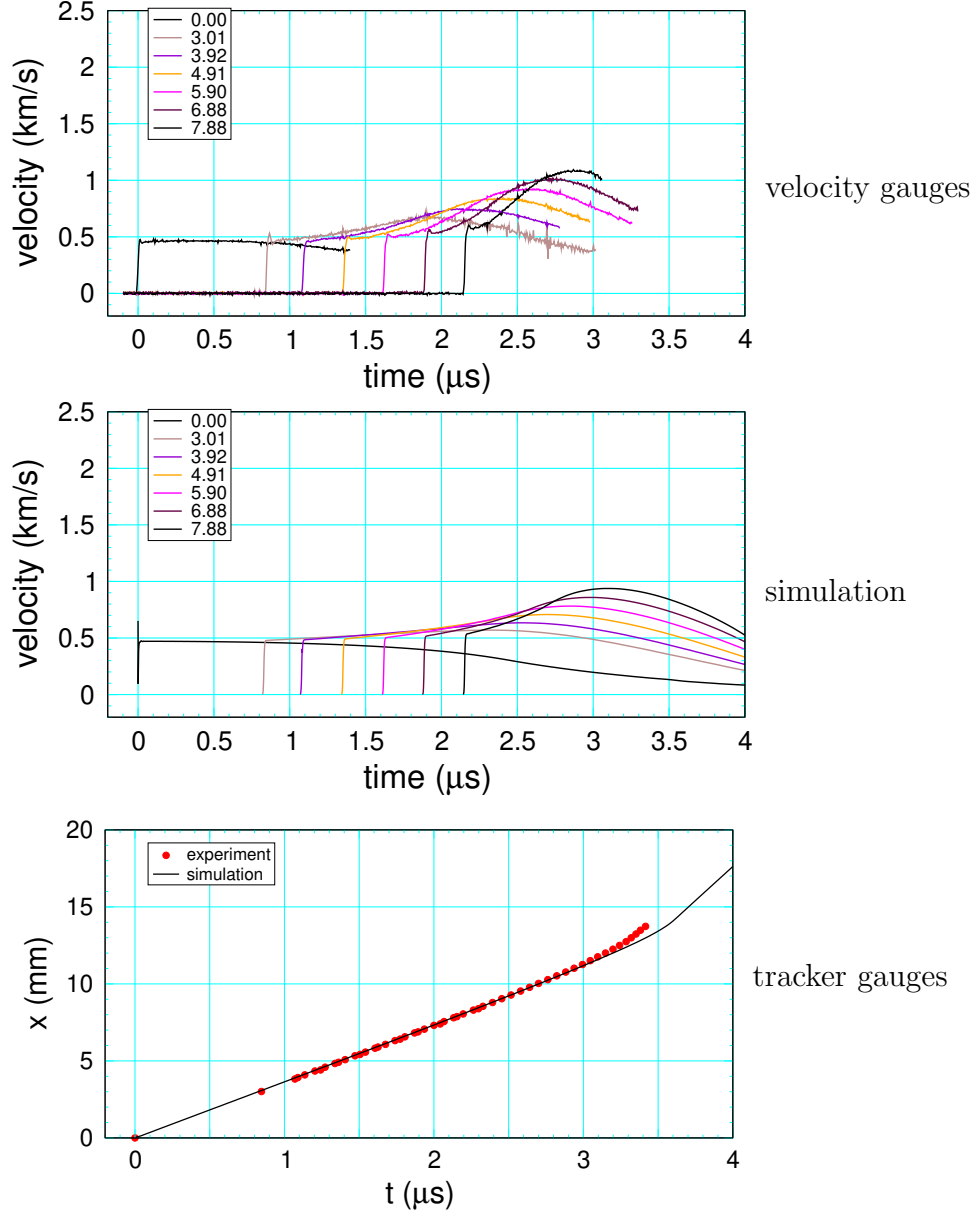


Figure 11: Comparison for shot 1s-1147 between experimental data [Gustavsen et al., 1999] and SURF model simulation. Top and middle plots for embedded velocity gauge data (legend labels gauge position in mm) and bottom plot for lead shock trajectory.

5 Curvature effect

Propagating detonation waves are characterized by the curvature effect; detonation speed as function of front curvature, $D_n(\kappa)$. It is determined from measurements of the axial detonation speed and front curvature of steady detonation waves. We use the fit to PBX 9501 rate stick experiment data given by [Aslam \[2007\]](#).

The slope of $D_n(\kappa)$ depends mostly on the reaction-zone width, hence the rate at high pressure; near P_{vn} , see fig. 2. Without the pressure ratio cutoff (see Appendix A) the rate would be too low and the curvature effect too large.

Rate stick simulations with a resolved reaction zone needed to calibrate parameters for the curvature effect would require very fine meshes (see fig. 3 and fig. 4) and be computationally expensive. Alternatively, the curvature effect can be computed from the quasi-steady reaction-zone profile ODEs; see [[Menikoff and Shaw, 2012](#), §2]. A comparison of the model and experimental curvature effects are shown in Figure 12.

Above $\kappa = 1.7 \text{ mm}^{-1}$, the ODEs do not have a solution. Usually, κ that large occurs at an HE interface. Due to the sonic boundary condition, the theory leading to the 1-D reaction-zone profile ODEs breaks down.

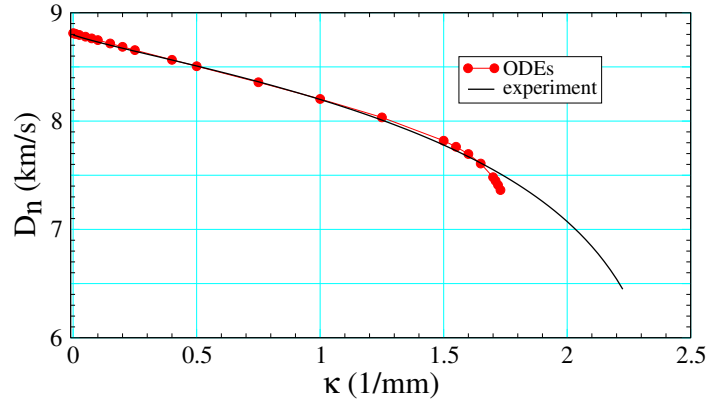


Figure 12: Curvature effect for SURF model based on quasi-stead profile ODEs [[Menikoff and Shaw, 2012](#), see §3] and experiment [[Aslam, 2007](#)].

Appendices

A SURF pressure ratio cutoff

The pressure ratio factor in Eq. (1b) is intended to help fit initiation experiments with more complex shock loading conditions than occurs for 1-D SDT experiments. In particular, the parameter n affects shock initiation with a pressure decreasing gradient behind the lead shock. A side effect is that it also increases the reaction-zone width for a propagating detonation wave. Hence, it increases the curvature effect; *i.e.*, the slope of $D_n(\kappa)$ increases.

To avoid the pressure ratio factor from affecting the detonation propagation regime the pressure ratio factor is cutoff at high pressures. For $p < p_s$, a cutoff function depending on p_s is introduced:

$$r_1(p_s) = \begin{cases} r_n & \text{for } p_s < p_1 , \\ \text{linear} & \text{for } p_1 < p_s < p_2 , \\ 1 & \text{for } p_2 < p_s , \end{cases} \quad (2)$$

where p_1 (pf_P1), p_2 (pf_P2) and r_n (pf_rn) are model parameters. Then the pressure ratio factor in Eq. (1b) $\left[\frac{p}{p_s}\right]^n$ is replaced with $\left[\max\left(\frac{p}{p_s}, r_1(p_s)\right)\right]^n$ for $p < p_s$.

Similarly for $p > p_s$, the cutoff function is

$$r_2(p_s) = \begin{cases} r_{nhi} & \text{for } p_s < p_1 , \\ \text{linear} & \text{for } p_1 < p_s < p_2 , \\ 1 & \text{for } p_2 < p_s , \end{cases} \quad (3)$$

where r_{nhi} (pf_rnhi) is an additional parameter. Then the pressure ratio factor is replaced with $\left[\min\left(\frac{p}{p_s}, r_2(p_s)\right)\right]^{nhi}$ for $p > p_s$.

In both cases the pressure ratio factor is 1 for $p_s > p_2$. By default $r_n = 0.5$ and $r_{nhi} = 2$. Reasonable values for parameters pf_P1 and pf_P2 are between the CJ pressure and the minimum pressure of the lead shock for a curved detonation wave, which maybe up to 30 percent less than the VN spike pressure. Lead shock pressures in this range are transitory and do not have much affect on reactive flow. For backwards compatibility, the old expressions are used if pf_P1 is the default value of 0.

B SURF rate parameters

xRage rate parameters for PBX 9501 using Davis reactants and Davis products EOS from [Aslam et al., 2020, tables I and II].

```
he_model(1)      = 6                ! SURF model
he_unreacted(1)  = REACTANTS        ! matid for Davis reactants
he_reacted(1)    = PRODUCTS         ! matid for Davis products

he_dtpct(1)      = 0.27             ! cfl number of detonation wave
he_zone_size(1)  = (0.012*$mm)      ! refine to zone_size
he_w_cutoff(1)   = 0                ! burn fraction cutoff
he_refine_dw(1)  = 0.0001           ! dw for refinement
he_surf_Pburn(1) = (2*$GPa)         ! burn threshold for CJ detonation
!
he_pscale(1)     = (1*$GPa)         ! pressure scale for rate parameters
he_tscale(1)     = (1*$microsec)    ! time      scale for rate parameters
!
! f(Ps) fitting form 4
he_surf_P0(1)    = 1.5              ! units pscale
he_surf_Plow(1)  = 3.5              ! units pscale
he_surf_P1(1)    = 42.0             ! units pscale
he_surf_Phigh(1) = 70.0            ! units pscale
!
he_surf_C(1)     = 0.0108           ! units 1/tscale
he_surf_fn(1)    = 2.45             ! dimensionless
!
he_surf_n(1)     = 2.5              ! dimensionless
he_surf_nhi(1)   = 1.5             ! dimensionless
he_surf_s1(1)    = 2.0             ! dimensionless
!
! pressure ratio cutoff
he_surf_pf_P1 = 40                  ! units pscale
he_surf_pf_P2 = 45                  ! units pscale
```

References

- T. D. Aslam. Detonation shock dynamics calibration of PBX 9501. In *Shock Compression of Condensed Matter – 2007*, pages 813–816, 2007. URL <https://doi.org/10.1063/1.2833248>.
- T. D. Aslam, M. A. Price, C. Ticknor, J. D. Coe, J. A. Leiding, and M. A. Zonker. AWSO calibration for the HMX based explosive PBX 9501. In *AIP conference proceedings*, 2020. URL <https://doi.org/10.1063/12.0000891>.
- T. R. Gibbs and A. Popolato, editors. *LASL Explosive Property Data*. Univ. of Calif. Press, 1980. URL <http://lib-www.lanl.gov/ladcdmp/epro.pdf>.
- R. L. Gustavsen, S. A. Sheffield, R. R. Alcon, and L. G. Hill. Shock initiation of new and aged PBX 9501 measured with embedded electromagnetic particle velocity gauges. Technical Report LA-13634-MS, Los Alamos National Lab., 1999. URL <https://doi.org/10.2172/10722>.
- L. G. Hill, C. E. Johnson, and D. N. Preston. Modeling the LANL gapstick experiment in PBX 9501 with the FLAG hydrocode. In *Proceeding of the Sixteenth International Symposium on Detonation*, page ?, 2018.
- R. Menikoff. SURFplus model calibration for PBX 9502. Technical Report LA-UR-17-31015, Los Alamos National Lab., 2017. URL <https://www.osti.gov/scitech/servlets/purl/1412839>.
- R. Menikoff. Simulating PBX 9501 Gapstick Experiment. Technical Report (in progress), Los Alamos National Lab., 2021.
- R. Menikoff and M. S. Shaw. The SURF model and the curvature effect for PBX 9502. *Combustion Theory and Modelling*, 16:1140–1169, 2012. URL <http://dx.doi.org/10.1080/13647830.2012.713994>.